

Epidemic dynamics with non-Markovian travel in multilayer networks

Yushu Chen ¹, Ying Liu ^{1,2}✉, Ming Tang ^{3,4}✉ & Ying-Cheng Lai ⁵

In our modern time, travel has become one of the most significant factors contributing to global epidemic spreading. A deficiency in the literature is that travel has largely been treated as a Markovian process: it occurs instantaneously without any memory effect. To provide informed policies such as determining the mandatory quarantine time, the non-Markovian nature of real-world traveling must be taken into account. We address this fundamental problem by constructing a network model in which travel takes a finite time and infections can occur during the travel. We find that the epidemic threshold can be maximized by a proper level of travel, implying that travel infections do not necessarily promote spreading. More importantly, the epidemic threshold can exhibit a two-threshold phenomenon in that it can increase abruptly and significantly as the travel time exceeds a critical value. This may provide a quantitative estimation of the minimally required quarantine time in a pandemic.

¹School of Computer Science, Southwest Petroleum University, 610500 Chengdu, P. R. China. ²Big Data Research Center, University of Electronic Science and Technology of China, 610054 Chengdu, P. R. China. ³School of Physics and Electronic Science, East China Normal University, 200241 Shanghai, China. ⁴Shanghai Key Laboratory of Multidimensional Information Processing, East China Normal University, 200241 Shanghai, China. ⁵School of Electrical, Computer and Energy Engineering, Arizona State University, Tempe, AZ 85287, USA. ✉email: shinningliu@163.com; tangminghan007@gmail.com

Epidemic spreading on networks has been an active research area in modern network science. Earlier, the interplay between epidemics and network structures was a focus^{1–4}. Human behaviors are then recognized as a major factor affecting the epidemic trajectories on local and global scales^{5–8}. Among the diverse behaviors, human mobility is key to disease spreading⁹. From the daily short-term commuters in large metropolitan areas to long-range travel via flights, trains, and buses, human mobility^{10–12} plays a key role in shaping the spatiotemporal patterns of global epidemics^{13–15}. Indeed, the modern transportation infrastructures of varying scales have made human beings much more connected^{16,17}. Infectious diseases thus propagate unprecedentedly faster and more widely and can evolve into a global pandemic¹⁸. For example, the rapid spread of SARS-CoV-2 all over the world leading to the COVID-19 pandemic can largely be attributed to travel¹⁹.

In terms of mathematical modeling, a number of frameworks are presently available for studying the impacts of human mobility on epidemic spreading, e.g., metapopulation network dynamics at the population level and multilayer networks at the individual level. In a metapopulation network, nodes represent subpopulations such as communities, cities, or countries, whereas edges between nodes describe human mobility between two subpopulations and the edge weights characterize the scale or strength of human mobility²⁰. Epidemic spreading among the subpopulations can be modeled as reaction-diffusion and reaction-commuting processes^{21–25}, where the reaction process describes the infection dynamics within the subpopulations, diffusion and commuting represent the mobility of population among the nodes. In this type of model, infected populations move and carry pathogens between the nodes, leading to an outbreak of infectious disease at the scale of the whole system. An example is the modeling of the COVID-19 pandemic, where models based on the metapopulation networks were developed to fit and predict the spreading trajectories and to evaluate the effects of different non-pharmaceutical interventions^{15,26}. At the individual level, multilayer networks have been used to study the impacts of mobility on epidemic spreading^{27,28}. In a multilayer network, the layers represent different types of connections among nodes, such as social contacts of individuals in different cities or on different social platforms, transportation by different modes, and different types of financial business among banks^{17,29}, where the dynamical interplay and couplings between the layers can alter the global epidemic threshold and the spreading dynamics^{3,30,31}.

While human mobility has been recognized as an important factor in modeling epidemic spreading in society, the roles of infection and recovery during travel that make the process fundamentally non-Markovian have not been addressed. It was recognized that infectious diseases can be transmitted and spread during air or land travel^{32–34}, which not only changes the spatial distribution of the hosts but also accelerates the spreading process and increases the total size of infection³⁵. Based on the human mobility data, models that incorporate the infection during travel can predict the evolution and peaks of the pandemic well^{36–38}. In these works, the travel process was assumed to be “instantaneous” without any memory effect. In particular, travel between different regions was modeled by a rate parameter—the probability that individuals start from one region and arrive in another, and the future occurrence can be predicted based solely on the present state of the system. Mathematically, such a process is said to be Markovian. However, many human activities, from communications to mobility, are not memoryless, which should be modeled as non-Markovian processes^{39–41}. In network epidemics, a non-Markovian process with memories can significantly alter the spreading dynamics^{42–46}. When individuals conduct a long-

distance journey, they may travel by flights, trains, buses or boats. During travel, infections can occur when travelers take the same transportation means with similar departure and arrival times. It takes a certain amount of time for the travelers to contact and infect each other during the travel process. Meanwhile, when a pandemic breaks out, such as COVID-19, travelers may be quarantined for a period of time when arriving in a new city, a new district, or a country. These observations suggest the necessity to treat travel with infections as a non-Markovian dynamical process. To our knowledge, incorporating non-Markovian travel dynamics into the epidemic spreading model represents a knowledge gap in the field. The purpose of our work is to fill this gap.

This paper presents a comprehensive treatment of epidemic spreading dynamics incorporating non-Markovian travel in multilayer networks. For simplicity, we consider a double-layer system, where infection and recovery occur both within the layers and during the travel between the layers. We introduce a quantity to characterize the non-Markovian travel process: the travel age that records the time a traveler is in transit. In particular, a traveler is exposed to contact with other travelers but only of the same travel direction and travel age. When the travel age is equal to the time required to arrive at the destination, the trip is regarded as completed. Based on the quenched mean-field theory (QMF), we derive the non-Markovian dynamical equations to describe the spreading dynamics in the double-layer system. We find that travel infections do not necessarily promote the spreading in the whole system in the sense of a reduced epidemic threshold but, counter-intuitively, can even increase it under different travel strengths (see below for a definition). An optimal travel strength can emerge at which the epidemic threshold reaches a maximum. Strikingly, with an increase in the travel time between the layers, the epidemic threshold first decreases and then enters a two-threshold region where, due to the recovery of the infected individuals during the travel, the outbreak size of the epidemic with a small infection rate is larger than that of an epidemic with a large infection rate. When the travel time is sufficiently large (e.g., with quarantine), the epidemic threshold finally reaches a high value. The time at the onset of the high threshold value can be taken as the minimally required time for quarantine. It is worth emphasizing that, in the Markovian travel model, only the outbreak peak is reduced as the travel time increases, while the outbreak time and the epidemic duration rarely change. In contrast, non-Markovian travel will result in a higher epidemic threshold, a delayed outbreak time and a longer epidemic duration. Our results thus justify that, for our simple model with non-Markovian travel, by increasing the travel time or the quarantine time, one can flatten the infection curve to mitigate the epidemic.

Results

Epidemic spreading model with travel infections. We articulate an epidemic spreading model supported on a double-layer networked system with non-Markovian travel infections. The system hosts two kinds of individuals: permanent residents in each layer and travelers; permanent residents stay within the layer, and travelers can either stay within a layer or travel between the layers along the interlayer edges. Permanent residents have connections only in their local layer, while travelers have connections in both layers. For travelers, the network connections within a layer are activated only when they are in that layer. Travelers can make contact with others and spread the disease within the layers and during the travel.

Figure 1 presents a schematic diagram of our non-Markovian model, where the networks in layers A and B have the same size

N . Each traveler generates an interlayer link. Let mN be the number of travelers in the system, where $0 < m < 1$. The total number of individuals in the network layers is then $N_{\text{tot}} = (2 - m)N$. At each time step, a number of travelers from layer A (B) initiate their trip at the rate q_A (q_B) and then travel along the interlayer link $A \rightarrow B$ ($B \rightarrow A$). For simplicity, we set $q_A = q_B = q$. Travelers who travel in the same direction and have the same travel age can contact with each other at the probability α . The time travelers have spent on the trip is their travel age l . When the travel age l equals the travel time t_T —the total time required to arrive at the destination layer since starting a trip (including quarantine time, if any), the trip is completed. For simplicity, we use a fixed value of α for the travel time and quarantine period. However, in reality, the contact rates should be different for travel and quarantine periods, where the contact rate in quarantine should be relatively low in a controlled environment. As the travelers take a certain time to arrive at the destination layer, the memory effect is naturally integrated into the model, making the process non-Markovian. (In contrast, for a Markovian travel process, the travelers would jump to the destination layer instantaneously⁴⁴ at the rate $1/t_T$. In this case, since there is no travel age, all travelers on the trip contact with each other at the rate α/t_T .)

In the real world, the number of travelers between two cities is generally stable over a long period of time, while an epidemic typically occurs in an abrupt manner. It is thus reasonable to assume in our model that the distribution of travelers between the two layers has reached a steady state before the epidemic begins. We use the standard SIR model to describe the spreading dynamics within each layer and on the trip, where a node can be in one of the three states: susceptible (S), infected (I) and recovered (R). At each time step, an I -node contacts and transmits disease to its susceptible neighbors at the rate β (the infection rate) and then transitions to the R -state at the rate μ (the recovery rate). Nodes in the R -state will not be infected anymore

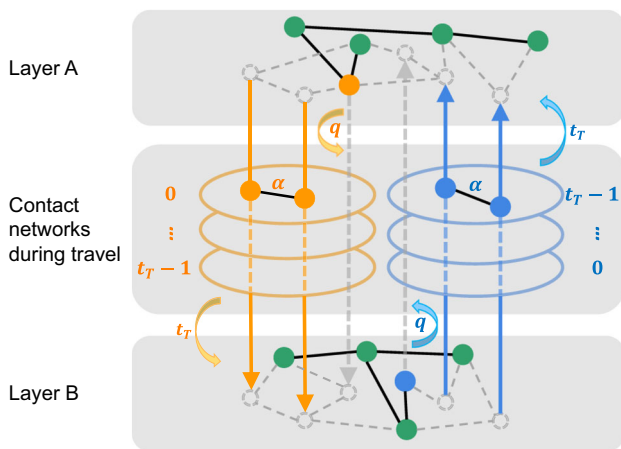


Fig. 1 Schematic illustration of the proposed epidemic spreading model with non-Markovian travel infections. There are four types of nodes in the network: the layer permanent residents (green solid circles), travelers in layer A or on the $A \rightarrow B$ interlayer links (yellow solid circles), travelers in layer B and on the $B \rightarrow A$ interlayer links (blue solid circles), and the nodes left by the travelers (open circles). A traveler has a pair of nodal positions, one in each layer, which are connected by an interlayer link. When travelers stay in a layer, they can contact with their neighbors within the layer (solid lines within each layer). Otherwise, their connections are deactivated (dashed lines in both layers). Travelers departing from the same layer at the same time form a fully connected subnetwork during the trip with the contact rate α . Travelers will arrive at the destination layer when their travel age l equals the travel time t_T .

and remain in this state. The epidemic process terminates when there are no longer any I nodes in the system. An epidemic outbreak occurs when the infection rate β is greater than a critical value⁴⁷, denoted as the epidemic threshold β_c , and the outbreak size is the fraction of R nodes in the steady state. The epidemic threshold can be determined empirically by calculating the outbreak size^{31,48}: the threshold is the minimal value of the infection rate β at which the outbreak size exceeds a small but not insignificant value (0.01 in our work). For SIR spreading dynamics, the approach of discrete-time modeling has been extensively used⁴. In general, there are two types of state updating rules for individual nodes: synchronous and asynchronous updating. In synchronous updating, infection occurs first, followed by recovery^{3,49,50}. In this case, the order of events is definite: in one time step with interval Δt , a susceptible node i becomes infected with the probability $1 - (1 - \beta\Delta t)^{n_i}$ is the number of this node's infected neighbors. Then, all infected nodes recover with the probability $\mu\Delta t$. When $\mu\Delta t$ or Δt is sufficiently small, the discrete-time dynamics associated with synchronous updating approach those with the asynchronous updating rule^{51,52}. We use the synchronous updating method to simulate the spreading process, which requires careful parameter selection to ensure simulation accuracy⁵³.

Impacts of travel strength on epidemic threshold. We first study the impacts of travel strength on the spreading dynamics, where the travel strength is characterized by the fraction m and the travel rate q of the travelers. Figure 2a–c shows the change in the epidemic threshold as a function of the traveler fraction m for different travel time t_T , denoted as β_c^T . For $t_T = 1$, an optimal travel fraction arises ($m \approx 0.15$) at which the epidemic threshold is the highest, where β_c^T first increases and then decreases at $t_T = 1$, as shown in Fig. 2a. This behavior can be understood by noting that the departure of the travelers reduces the mean active degree within each layer, thereby leading to an increase in the epidemic threshold, while contacts during the trip promote the infections among the travelers so as to reduce the threshold. As a comparison, we calculate the epidemic threshold β_c^H of a two-layer system with travelers hopping between layers but without travel infections³¹, as well as the epidemic threshold β_c^S for a single-layer network. Without travel infections, the threshold β_c^H increases monotonically with m and is larger than β_c^T and β_c^S , as the result of reduced contacts and infections within the layers due to the travel. When travel infections are taken into account, the epidemic threshold β_c^T first increases and then decreases to values smaller than that of the single layer. For $t_T = 4$, β_c is nearly constant for $m < 0.1$ and then decreases rapidly for $m > 0.1$, as shown in Fig. 2b. For $t_T = 16$, the epidemic threshold β_c^T reaches a local maximum at $m \approx 0.5$, as shown in Fig. 2c. These results indicate that travel infections can have a significant effect on the dynamics with a complicated dependence of the epidemic threshold on the travel time.

Figure 2d–f shows the epidemic threshold versus the travel rate q for three different values of the travel time t_T : $t_T = 1, 4$, and 16 , respectively. For $t_T = 1$ [Fig. 2d] and 4 [Fig. 2e], β_c^T decreases with q initially but tends to a constant (approximately) for $q \gtrsim 0.5$. The initial decrease in the epidemic threshold is the result of increasing contact among travelers as more individuals begin to travel, thereby promoting the disease spreading. However, when the travel rate q becomes large, the travelers do not stay in one layer for a relatively long time, so the spreading dynamics in each layer are suppressed. For a sufficiently long travel time, e.g., $t_T = 16$ [Fig. 2f], the threshold is hardly impacted by the travel rate q .

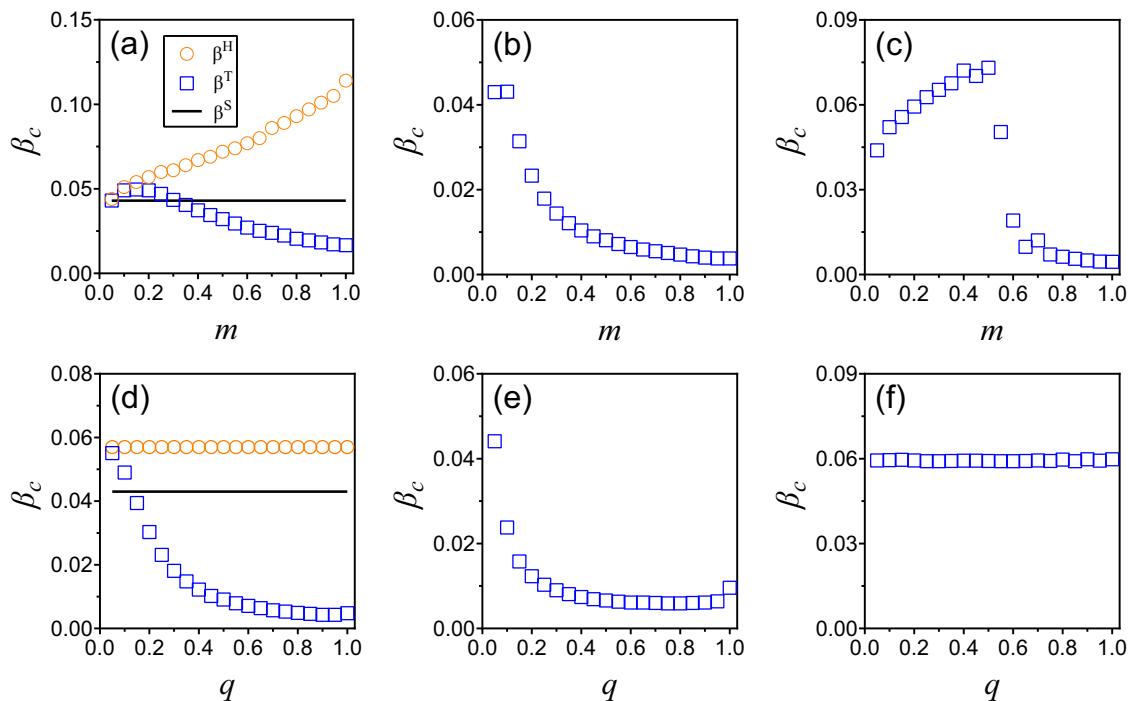


Fig. 2 Dependence of epidemic threshold on the travel strength. **a–c** Epidemic threshold as a function of traveler fraction m for $t_T=1, 4$, and 16 , respectively, for $q=0.1$. In **(a)**, β_c^T (blue squares), β_c^H (orange circles), and β_c^S (the gray line) are the epidemic thresholds from the model with travel infections, the interlayer hopping model without travel infections, and a single-layer network, respectively. The increase of β_c^T with m is due to the departure of the travelers from each layer, which is larger than β_c^S . The threshold β_c^T first increases and then decreases with m , where the former is due to the departure-induced reduction of infection in each layer, and the latter is caused by travel infections. For a long travel time, β_c^T exhibits a peak **(c)**. **d–f** Epidemic threshold versus the travel rate q for $t_T=1, 4$ and 16 , respectively, for $m=0.2$. Other parameters are $\alpha=1$ and $\mu=0.5$. Each layer is an ER random network with size $N=1 \times 10^4$ and average degree $\langle k \rangle=10$. Each data point is averaged over 10^3 network realizations.

The behaviors in Fig. 2a–f entail that the impacts of different m and q values on the epidemic threshold can be understood in terms of the contact activities. Especially for a fixed q value, an optimal m value can emerge at which the epidemic threshold is the highest (see Supplementary Note 1 for details). We have also studied double-layer network configurations with the heterogeneous ER-SF (scale-free) and SF-SF combinations and obtained similar results (Supplementary Note 2).

Impacts of travel time on epidemic spreading dynamics.

Figure 2a–f illustrates that the dependence of the epidemic threshold on the traveler fraction m and travel rate q can vary with the travel time t_T resulting from, e.g., different transportation modes (airplane, train, or boat). Since the hallmark of non-Markovian travel is a finite travel time in our model, it is useful to investigate the effects of the travel time t_T on the spreading dynamics. Figure 3a, b shows how the steady-state outbreak size $R(\infty)$ is affected by t_T and the infection rate β . In particular, Fig. 3a reveals that, for $\beta=0.1$, the outbreak size decreases with t_T . However, for $\beta=0.02$ or $\beta=0.04$, $R(\infty)$ first increases and then decreases with t_T . Figure 3b shows that the dependence of $R(\infty)$ on β also varies for different values of t_T . For example, for $t_T=8$, $R(\infty)$ first increases and then decreases toward an approximately near zero value but finally increases rapidly with β . The results in Fig. 3a, b suggest rather complex impacts of the travel time on the spreading dynamics.

To understand the impact of non-Markovian travel on the spreading dynamics, we have developed a theoretical framework based on the quenched mean-field (QMF) approximation (see “Methods”). Figure 3c, d presents the theoretically predicted and numerically calculated phase diagram of the steady-state infection size $R(\infty)$, respectively, in the parameter plane (t_T, β) . In Fig. 3c,

we divide the diagram into three regions according to the travel time t_T : $t_T \in [1, 7)$, $t_T \in [7, 12]$ and $t_T \in (12, 20]$. In the first region, $R(\infty)$ increases with the infection rate β . In the second region, $R(\infty)$ first increases with β , and the epidemic breaks out at the first threshold. The infection size then decreases with β to a small value under 0.01. The epidemic breaks out again as β increases through a second threshold, and $R(\infty)$ continues to increase with β afterward. This is a two-threshold phenomenon due to the interplay between the infection and recovery of the travelers during the travel process where, when β varies between the two thresholds, the infection size with a low infection rate is larger than that associated with a high infection rate. In the third region, where the travel time is relatively long, the infection size first increases slowly with β and remains small for a large range of β . When β is sufficiently large, an outbreak occurs, and $R(\infty)$ increases with β . In spite of the slightly larger theoretical value of $R(\infty)$ due to the “echo chamber” effect in solving the dynamical evolution equations⁵⁴, there is a general agreement between the theoretical and numerical results.

The two-threshold phenomenon illustrated in Fig. 3 is the result of the recovery involved in the non-Markovian travel dynamic, which can either promote or suppress epidemic in the whole double-layer system. In particular, the black dashed line in Fig. 3c, d represents the epidemic threshold when there is only infection but no recovery (recovery rate $\mu=0$) during the travel, which agrees with the low epidemic threshold predicted by the QMF theory. The low threshold decreases with t_T , indicating that the travel infections promote epidemic spreading in the system. The black dash-dotted line represents the epidemic threshold when there are contacts and infections only at the first time step in the travel process, while in the remaining t_T-1 time steps, there is only recovery. This corresponds to the real-world

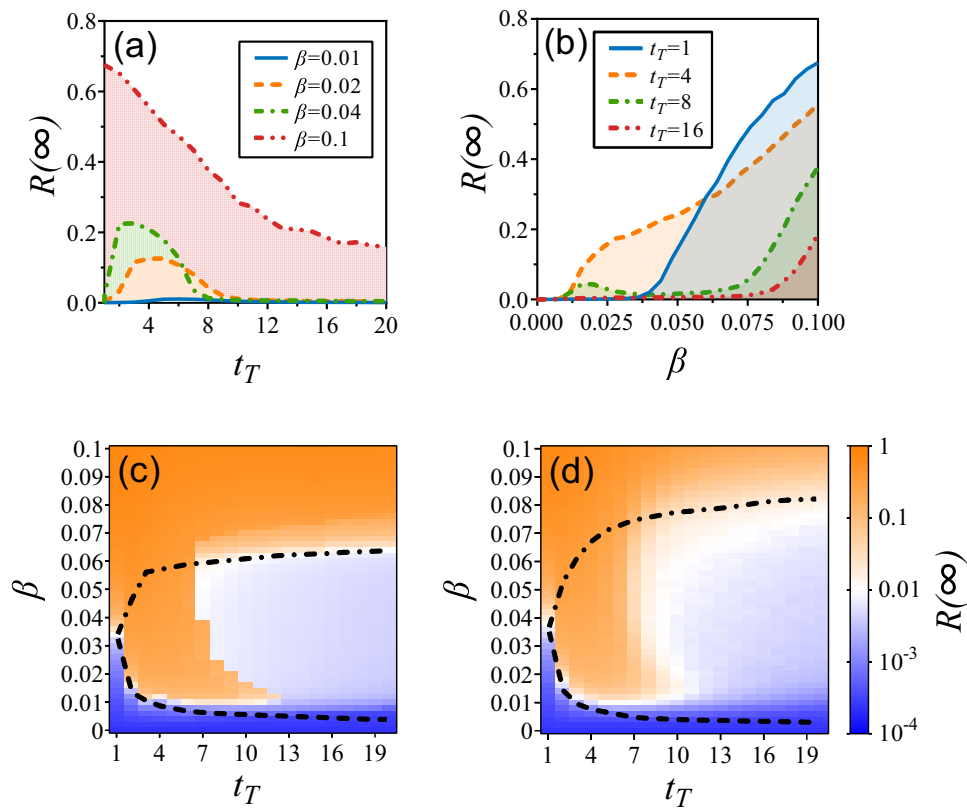


Fig. 3 Dependence of epidemic outbreak size on travel time and infection rate. Outbreak size versus **a** the travel time t_T for different values of the infection rate and **b** the infection rate β for different travel times. **c** Theoretical prediction and **d** the corresponding numerical results of the final infection size $R(\infty)$ shown as color-coded values in the parameter plane (t_T, β) . For $t_T > 1$, a two-threshold phenomenon arises, where the black dashed line in each panel represents the epidemic threshold when there is only infection but no recovery during the travel, and the black dash-dotted line denotes the epidemic threshold when infection occurs only once—at the first time step during the travel, while there is only recovery for the remaining travel time, a situation that arises when a mandatory quarantine is imposed at the travel destination. The emergence of the second (higher) threshold can thus be interpreted as the result of quarantine. Other parameters are $m = 0.4$, $q = 0.1$, $\alpha = 1$ and $\mu = 0.5$. Each layer is an ER network of size $N = 1 \times 10^4$ and average degree $\langle k \rangle = 10$. Each data point is the result of averaging over 10^3 statistical realizations.

situation where travelers are quarantined for a period of time when they arrive at their destinations. In this case, increasing the travel time (quarantine time) can result in an increase in the epidemic threshold that agrees with the high epidemic threshold predicted by our theory, indicating that travel recovery suppresses the epidemic spreading in the whole system.

To understand how the infection within the layers and during travel affect the outbreak size of the entire system, we calculate and analyze the numbers of two types of individuals: the cumulative numbers of individuals infected within the layers and during the travel, denoted as n_{LL} and n_{EE} , respectively. We also calculate the number n_{EL} of the infected individuals switching from the travel process to the layers and the cumulative number n_{LE} of the infected individuals transitioning from layers to the interlayer edges. (Details of how n_{LL} , n_{EE} , n_{EL} and n_{LE} are calculated are given in Supplementary Note 3). We also find that the critical (small) t_T value at which the two-threshold phenomenon disappears is mainly determined by the recovery rate μ , where a large value of μ leads to a small critical t_T (Supplementary Note 4). The reason is that if the infected individuals are able to recover in a short time, they will have sufficient time to recover during the trip, even when the travel time t_T is small. Furthermore, when the contact ability α during travel reduces to values less than one, insofar as the contacts between travelers are more frequent than those within each layer, the two-threshold phenomenon persists (see Supplementary Note 4 for details), where the low threshold increases as α

decreases. The phenomenon ceases to exist but only when α is reduced to a quite small value, e.g., 0.1, where the average degrees of the contact network during travel and of the layer are equal. It is worth noting that such small values of α are not physically meaningful, as the contacts during travel are typically much more frequent than those within a layer in our model, which is the case for respiratory disease and in large-capacity public vehicles such as trains and airplanes. In addition, we preliminarily explore the impact of the restricted number of contacts during travel on the two-threshold phenomenon, as is detailed in Supplementary Note 5. It is found that the two-threshold phenomenon may be susceptible to the risk of interlayer infection and becomes more obvious with increasing the network size. However, it is also necessary to explore the impact of the restricted number of contacts during travel on the epidemic dynamics in multilayer networks, especially to find out whether all the results are finite size-dependent and do hold in the thermodynamic limit.

Figure 4 presents the time evolution of the prevalence $\rho(t)$ for different values of the infection rate β . For low infection rates ($\beta = 0.02$ in Fig. 4a and $\beta = 0.04$ in Fig. 4b), multiple outbreak peaks arise. In this case, the epidemic does not break out in the layers [Supplementary Fig. 4c in Supplementary Information]. On the contrary, travelers with the same travel age and direction are fully connected during the trip, leading to an outbreak and an increase in $\rho(t)$. When some travelers have arrived at the destination layer, $\rho(t)$ decreases because the infection rate is too small to induce an outbreak within the layer. However, when the

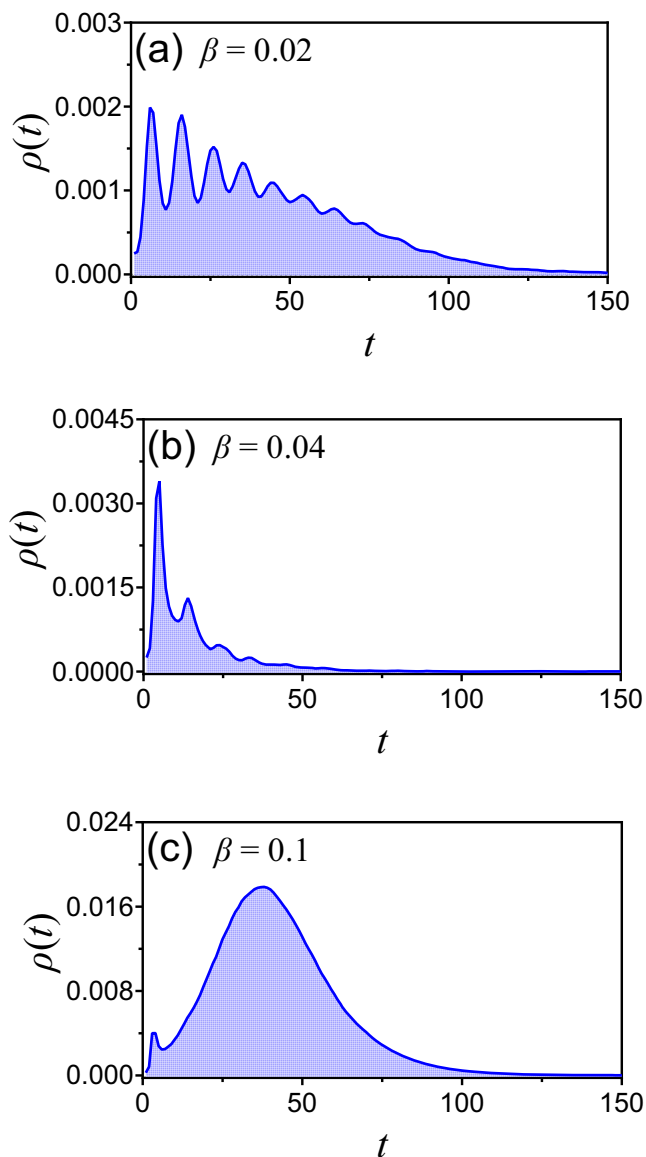


Fig. 4 Time evolution of prevalence. Shown is the evolution of $\rho(t)$ for **a** $\beta = 0.02$, **b** $\beta = 0.04$ and **c** $\beta = 0.1$. The travel time is $t_T = 8$. The distinct feature is the occurrence of multiple peaks in $\rho(t)$ during its time evolution —see text for details. Other parameter values are $m = 0.4$, $q = 0.1$, $\alpha = 1$ and $\mu = 0.5$.

travelers start to travel again, $\rho(t)$ can increase. The non-Markovian travel process with the memory effect well captures the feature of the multiple peaks when travel infections dominate the epidemic dynamics in the system. For $\beta = 0.04$, since the infection and recovery are faster than those for $\beta = 0.02$, the number of infections arriving at the destination layer decreases. This results in a rapid decrease in the subsequent infection peaks. For $\beta = 0.1$ [Fig. 4c], infections can break out both within the layers and during the travel, so ρ first increases and then decreases. For $t \approx 4$, a small peak in ρ arises due to the fact that, during a few initial time steps, infections within the layers have not broken out, and they mainly come from the travel process.

Comparison with Markovian travel process. To emphasize the fundamental importance of non-Markovian travel in epidemic spreading, we carry out a comparison study of the spreading dynamics with Markovian and non-Markovian travel. Figure 5

shows that, due to the memory effects in travel infections, non-Markovian travel leads to a higher epidemic threshold than that with Markovian travel. In particular, in a non-Markovian travel process, only travelers with the same travel age and direction can form a connected network to spread the disease, which lasts for a time length of t_T . However, for a Markovian travel process, infected individuals can contact with all other travelers and return to the layer at the rate $1/t_T$, while the infected individuals remaining in the travel state can continue to infect other travelers, which in turn promote the infections in the layers. Note that, for both types of travel, the epidemic threshold decreases with m [Fig. 5a] and q [Fig. 5b], indicating that travel, in general, promotes epidemic spreading. When q is large, β_c with non-Markovian travel increases. This is because travelers cannot stay in one layer for a relatively long time, which in turn suppresses the epidemic spreading in each layer. The change of the epidemic threshold with m and q at different t_T is analyzed in Supplementary Note 6.

A remarkable phenomenon occurs for epidemics with non-Markovian travel, where the epidemic threshold remains low and nearly constant until the travel time exceeds a large critical value, at which an abrupt increase in the threshold occurs. A representative result is shown in Fig. 5c, where the epidemic threshold β_c versus the travel time t_T for both types of travel dynamics is displayed. For the non-Markovian process, β_c first decreases with t_T . When t_T varies in the range [7, 12], a two-threshold phenomenon occurs where, for a certain t_T , a small-scale epidemic breaks out at a low epidemic threshold. As the infection rate increases, the infection size decreases to a small value of about 0.01. Only when the infection rate increases through the second (higher) epidemic threshold will another outbreak become possible. For sufficiently long travel, e.g., $t_T > 12$, the epidemic threshold increases with t_T . A long travel time, in general, is the result of government-imposed quarantine, and Fig. 5c provides a quantitative criterion to determine the minimal quarantine time: quarantine must be sufficiently long to ensure that a high epidemic threshold is achieved! In the particular setting of Fig. 5c, the minimal quarantine time should be about $t_T \sim 12$. It should be noted that, in the Markovian travel model, travel between the network layers is an instantaneous process that occurs at the rate $1/t_T$, so t_T here is a mere model parameter: it is not indicative of any kind of actual travel time. In this case, as shown by the orange circles and curve in Fig. 5c, β_c decreases rapidly for small t_T as travel promotes spreading and then starts to increase slowly because of the continuous reduction in the switching rate from the trip to the layers, implying that quarantine would have no effect in suppressing the epidemics and rendering invalid any model with Markovian travel.

We have also examined the time evolution of the prevalence ρ for different values of the infection rate β for the non-Markovian and Markovian travel models, as shown in Fig. 6a–d. It can be seen that the non-Markovian travel model has a lower infection peak, a delayed outbreak time, and a longer infection duration than that of the Markovian travel model. The difference can be quite significant, especially for small values of β , as shown in Fig. 6a because, in this case, the infections incurred during the travel are the main contributing factor to the epidemic in the whole system. The multiple outbreaks exemplified in Fig. 6a are the result of the memory effects associated with non-Markovian travel. As β increases, the epidemic can break out both within the layers and during travel, so the differences from the travel process become less significant, as shown in Fig. 6b, c, and exemplified in Fig. 6d. These results indicate that, compared with the more realistic non-Markovian travel model, the Markovian travel model overestimates the epidemic threshold and the infection peak but underestimates the spreading time. Furthermore, we

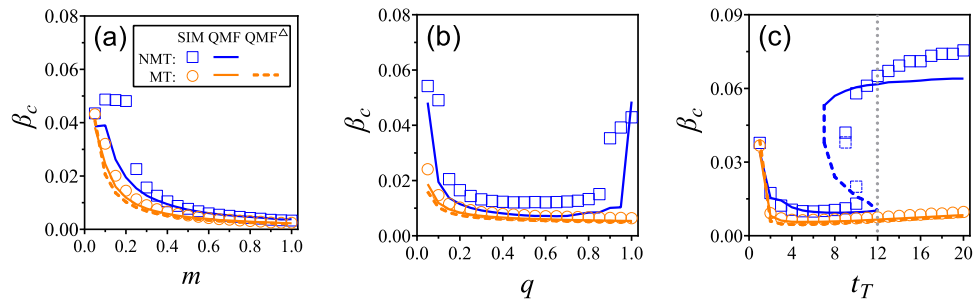


Fig. 5 Comparison between epidemic dynamics with non-Markovian and Markovian travel. Shown is the epidemic threshold β_c versus the traveler fraction m , the travel rate q , and the travel time t_T for non-Markovian travel and Markovian travel: **a** β_c versus m for $q = 0.1$ and $t_T = 8$, **b** β_c versus q for $m = 0.2$ and $t_T = 8$, and **c** β_c versus t_T for $q = 0.1$ and $m = 0.4$. In both cases, β_c decreases continuously with m and q . However, as the travel time increases, a two-threshold phenomenon occurs for the non-Markovian travel model: the threshold remains low until a critical time is reached, at which the threshold abruptly increases to a much larger value. This means that the epidemic is greatly suppressed if the travel time is longer than the critical time, providing a quantitative criterion to determine the necessary quarantine time to effectively suppress the epidemic because, after the quarantine, the infection rate needs to be much higher (possibly biologically infeasible) to lead to an outbreak. In stark contrast, the Markovian travel spreading model, by design, is unable to take quarantine into account, rendering it inapplicable to modeling real-world epidemics that involve travel. The symbols are numerical results, and the curves are the corresponding theoretical predictions from the dynamical equations (solid) and the Jacobian matrix method (dashed). Other parameters are set as $\alpha = 1$ and $\mu = 0.5$.

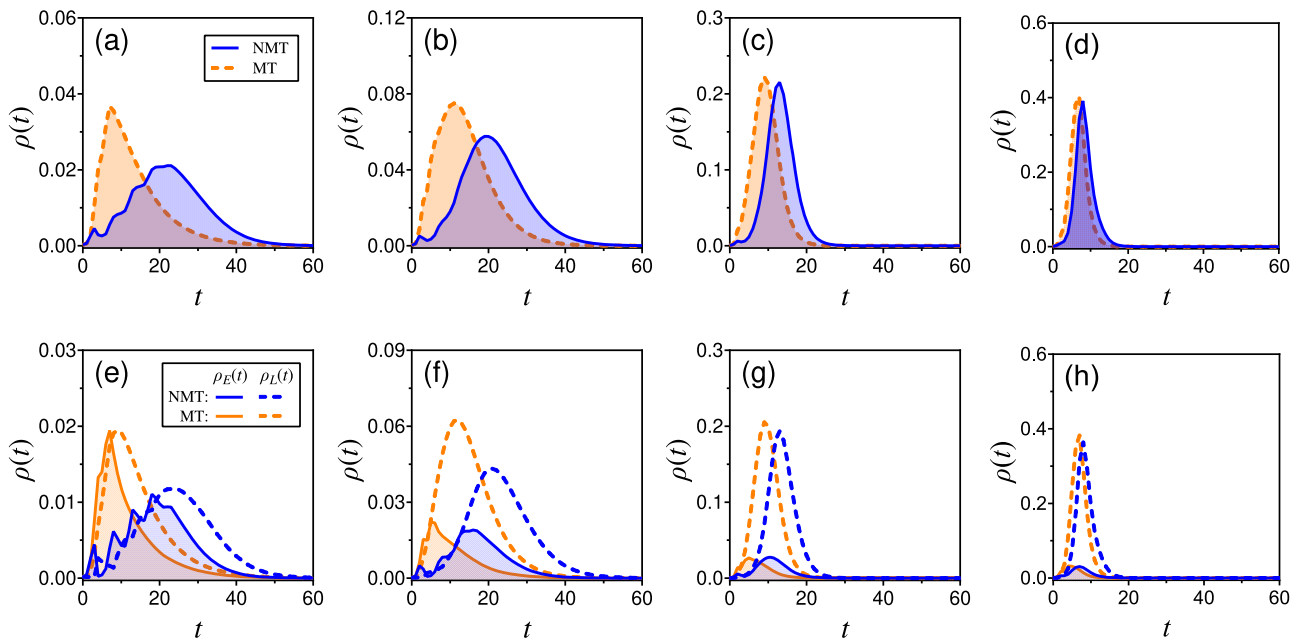


Fig. 6 Comparison of time evolution of prevalence between non-Markovian travel (NMT) and Markovian travel (MT) epidemic models. **a-d** Time evolution $\rho(t)$ and **e-h** time evolution of the layer prevalence $\rho_L(t)$ (dashed curves) and the travel prevalence $\rho_E(t)$ (solid curves) for $\beta = 0.05, 0.1, 0.2$, and 0.4 , respectively. Other parameters are set as $m = 0.4, q = 0.1, t_T = 4, \alpha = 1$ and $\mu = 0.5$.

find that increasing the travel time t_T leads to a reduced outbreak peak, a delayed outbreak time and a longer epidemic duration in the non-Markovian travel model, which are not found in the Markovian travel model, as shown in Supplementary information Note 6 (Supplementary Fig. 9). The non-Markovian travel model provides evidence for the effectiveness of travel time in moderating the development of epidemic.

Additional insights into the difference between the non-Markovian travel and Markovian travel epidemic dynamics can be gained by distinguishing the evolution of the prevalence from the layers and the travel process, denoted as $\rho_L(t)$ and $\rho_E(t)$, respectively. Figure 6e-h shows that, as the infection rate β increases from 0.05 to 0.4, the fraction of the infections from travel decreases, indicating that the effect of travel infections is more significant when the infection rate is small. Since, for non-Markovian travel, the travelers return to layers when their travel

age is t_T , multiple infection peaks in ρ_E can arise, as shown in Fig. 6e, where the highest peak is lower and occurs later than that from the Markovian travel model. For the Markovian travel model, infected individuals return to the layer at the rate $1/t_T$, and the remaining infected individuals in the travel process can continue to infect other travelers, leading to an earlier onset of the epidemic outbreak than that in the non-Markovian travel model. As β increases and the effects of travel infections decrease [Fig. 6f-h], the differences between the two travel models become less significant.

Discussion

In large-scale epidemic spreading such as the COVID-19 pandemic, travel is an indispensable and perhaps one of the most significant contributing factors. To properly incorporate travel into epidemics is essential to rendering the model predictions

relevant to the real world. Previous models taking travel into account used an overly simplistic approach: travel has been treated as a Markovian process without any memory effect, i.e., travel is assumed to occur instantaneously at a certain rate. Because of this idealization, issues pertinent to making travel policies and guidelines during the pandemic cannot be addressed by models with Markovian travel. To provide informed policies backed up by quantitative science, the non-Markovian nature of the travel process must be taken into account. For example, when a large epidemic occurs, an important issue is for the authorities to determine the minimal quarantine time based on quantitative model predictions. Our present work represents an initial step in this direction by developing a framework to incorporate realistic, non-Markovian travel into epidemic modeling. While there are many mechanisms by which a spreading process can become non-Markovian, e.g., through a non-exponential distribution of infectiousness, for spreading dynamics incorporating travel, an intuitive and reasonable way is to set a non-zero, constant travel time.

Our model is a two-layer network system, where travel between the layers is non-Markovian, a process that requires a finite amount of time to complete. In spite of the complexity introduced by the non-Markovian travel, the model is analytically tractable. Through mathematical analyses and extensive numerical simulations, our model captures a number of phenomena. First, due to the non-Markovian nature, travel infections do not necessarily promote the epidemic spreading in the system. In fact, there is an optimal travel strength at which the epidemic threshold reaches a maximum. Second, but more importantly, as the travel time increases, the epidemic threshold can exhibit a remarkable two-threshold behavior. In particular, when the travel time is below a critical value, the epidemic threshold is low, making a large-scale outbreak possible. The finding is an abrupt and significant increase in the threshold as the travel time exceeds the critical value. This means that to suppress the epidemic, the travel time should be longer than some critical value. Third, we have analyzed the effects of contact ability in the travel process and found that, for infectious diseases with a high infection rate, reducing the contact in travel is generally ineffective in suppressing the disease (Supplementary Note 7). Compared with epidemic models with the simplistic Markovian travel process, our non-Markovian model induces a higher epidemic threshold and a delayed outbreak time at the price of a longer infection period and also generates the real-world phenomenon of multiple infection peaks.

Our non-Markovian travel-based framework provides a complex network approach to addressing the role of human behaviors in spreading dynamics. The framework is demonstrated to be successful in capturing real-world phenomena, such as the effectiveness of quarantine strategy and the occurrence of multiple outbreak peaks as widely witnessed since the beginning of the COVID-19 pandemic. The emergence of a two-threshold region in the epidemic threshold with respect to the traveling time may provide a quantitative estimation of the necessary quarantine time for travelers. The delayed outbreak time and a longer epidemic duration in our non-Markovian model imply the effects of travel time and quarantine time on flattening the infection curve, where a moderate epidemic has the advantage of causing less stress on the healthcare system. The results of our comparative analysis have essentially denied the use of Markovian travel-based epidemic models to capture the role of real-world travel in epidemics. All these indicate the absolute necessity to use a non-Markovian process to incorporate human behaviors into epidemic modeling.

In our model, there are some simplifying assumptions, including a fixed travel time (as opposed to a distribution) to

characterize non-Markovian travel, the assumption of a fully connected network during trips, the adoption of Markovian epidemic spreading dynamics, and the absence of additional non-pharmacological interventions. A potential topic for future investigation is considering more realistic travel processes with larger-scale populations (such as metapopulation networks and agent-based models), where travel times exhibit a distribution and individual heterogeneity is taken into account. The traveler on trip should be further divided into different connected groups to represent that travelers will be within different vehicles of fixed capacity. Another open issue is to integrate travel infections into travel-based non-pharmaceutical interventions aimed at effective epidemic control. Introducing non-Markovian travel into more realistic models holds promise for yielding meaningful outcomes distinct from previous findings.

Methods

Matrix to describe node positions. QMF is an individual-based mean-field method, where the adjacency matrix of the network is integrated to calculate the probability of each individual being in any one of the possible states⁴. To describe the spreading dynamics on a multilayer network with interlayer travel infections, we define a supra-adjacency matrix G_C of size $4N \times 4N$ to describe the contacts between individuals in the system, which is

$$G_C = \begin{bmatrix} G_A & 0 & 0 & 0 \\ 0 & G_E & 0 & 0 \\ 0 & 0 & G_E & 0 \\ 0 & 0 & 0 & G_B \end{bmatrix},$$

where G_A and G_B are the adjacency matrices characterizing the contacts in layers A and B , respectively, and G_E is the contact matrix of travelers during the trip [$e_{ij} = 1$ if both i and j ($i \neq j$) are travelers, otherwise $e_{ij} = 0$]. Different from a network adjacency matrix, c_{ij} in matrix G_C represents the possible contact between the individuals at positions i and j . These positions can be the nodal positions in layers A and B , and they can also be on the interlayer edges $A \rightarrow B$ and $B \rightarrow A$. Specifically, $i \in [1, N]$ indicates that it is a nodal position in layer A , $i \in [N + 1, 2N]$ signifies that the node is located on the interlayer edge $A \rightarrow B$, $i \in [2N + 1, 3N]$ specifies a node on the interlayer edge $B \rightarrow A$, and $i \in [3N + 1, 4N]$ gives that the node is in layer B . For the travelers to form the contact network on the trip, they must have the same travel age and directions (the distribution of the travelers at different locations is analyzed in Supplementary Note 8). The average degree of the contact network depends on the total number of travelers, the contact ability and the travel time, as stipulated by Eq. (S3).

To describe the impacts of travel behaviors of individuals, we define the following travel matrix G_H :

$$G_H = \begin{bmatrix} -G_T & 0 & G_T & 0 \\ G_T & -G_T & 0 & 0 \\ 0 & 0 & -G_T & G_T \\ 0 & G_T & 0 & -G_T \end{bmatrix},$$

where each row of the matrix quantifies the travel-induced change (due to the departure and arrivals of the travelers) in the active nodes at the nodal positions in layer A , trip from A to B , trip from B to A , and the positions in layer B , respectively. The matrix G_T is diagonal with the size $N \times N$, where $t_{ii} = 1$ if node i is a traveler, otherwise $t_{ii} = 0$. Let $H_{i,j}$ denote the elements of G_H . The relation $H_{1,1} = -G_T$ means that the departure of travelers from layer A will reduce the number of active nodes in layer A , and $H_{1,3}$ represents that travelers along the interlayer edge $B \rightarrow A$ to layer A will increase the number of active nodes in layer A .

Similarly, $H_{2,2}$, $H_{3,3}$ and $H_{4,4}$ represent the decrease in the active nodes due to the departure of travelers from $A \rightarrow B$, $B \rightarrow A$ and layer B , respectively, and $H_{2,1}$, $H_{3,4}$ and $H_{4,2}$ represent the increase in the active nodes due to the arrival of the travelers at $A \rightarrow B$, $B \rightarrow A$ and layer B , respectively. To facilitate the derivation of the dynamical equations and theoretical analyses, we divide G_H into two matrices: G_F and G_D given by

$$G_F = \begin{bmatrix} 0 & 0 & G_T & 0 \\ G_T & 0 & 0 & 0 \\ 0 & 0 & 0 & G_T \\ 0 & G_T & 0 & 0 \end{bmatrix},$$

and

$$G_D = \begin{bmatrix} -G_T & 0 & 0 & 0 \\ 0 & -G_T & 0 & 0 \\ 0 & 0 & -G_T & 0 \\ 0 & 0 & 0 & -G_T \end{bmatrix}.$$

Spreading dynamics in multilayer network with Markovian travel. We define $s_i(t)$, $\rho_i(t)$ and $r_i(t)$ as the probabilities of a position i holding an individual being in state S , I and R at time t , respectively, where i represents one of the nodal positions in layer A , $A \rightarrow B$, $B \rightarrow A$ and layer B , as in matrices G_C and G_H . Permanent residents stay in one of the layers, and travelers can be in one of the four possible positions. Let p_i be the probability of the nodal position i being active (an individual is actually there). The details involved in the calculation of p_i can be found in Supplementary Note 8. As an individual can be in one of the three possible disease states, we have $s_i(t) + \rho_i(t) + r_i(t) = p_i$. As the individuals within the layers and on the travel process have different spreading dynamics, we divide the nodes into two groups: $\Omega_L = \{i | i \in [1, N] \cup [3N + 1, 4N]\}$ and $\Omega_E = \{i | i \in [N + 1, 3N]\}$, representing, respectively, the sets of nodes within layers and on the interlayer edges. The set of differential equations describing the spreading dynamics in the multilayer system with Markovian travel infections can then be written as

$$\frac{ds_i(t)}{dt} = \begin{cases} -s_i(t)\lambda_i(t) + q \sum_{j=1}^{4N} d_{ij} (1 - \lambda_j(t)) s_j(t) \\ + \frac{1}{t_r} \sum_{j=1}^{4N} f_{ij} (1 - \lambda_j(t)) s_j(t), & i \in \Omega_L; \\ -s_i(t)\lambda_i(t) + \frac{1}{t_r} \sum_{j=1}^{4N} d_{ij} (1 - \lambda_j(t)) s_j(t) \\ + q \sum_{j=1}^{4N} f_{ij} (1 - \lambda_j(t)) s_j(t), & i \in \Omega_E, \end{cases} \quad (1)$$

$$\frac{d\rho_i(t)}{dt} = \begin{cases} s_i(t)\lambda_i(t) - \mu\rho_i(t) + q \sum_{j=1}^{4N} d_{ij} [(1 - \mu)\rho_j(t) + s_j(t)\lambda_j(t)] \\ + \frac{1}{t_r} \sum_{j=1}^{4N} f_{ij} [(1 - \mu)\rho_j(t) + s_j(t)\lambda_j(t)], & i \in \Omega_L; \\ s_i(t)\lambda_i(t) - \mu\rho_i(t) + \frac{1}{t_r} \sum_{j=1}^{4N} d_{ij} [(1 - \mu)\rho_j(t) + s_j(t)\lambda_j(t)] \\ + q \sum_{j=1}^{4N} f_{ij} [(1 - \mu)\rho_j(t) + s_j(t)\lambda_j(t)], & i \in \Omega_E, \end{cases} \quad (2)$$

$$\frac{dr_i(t)}{dt} = \begin{cases} \mu\rho_i(t) + q \sum_{j=1}^{4N} d_{ij} (r_j(t) + \mu\rho_j(t)) \\ + \frac{1}{t_r} \sum_{j=1}^{4N} f_{ij} (r_j(t) + \mu\rho_j(t)), & i \in \Omega_L; \\ \mu\rho_i(t) + \frac{1}{t_r} \sum_{j=1}^{4N} d_{ij} (r_j(t) + \mu\rho_j(t)) \\ + q \sum_{j=1}^{4N} f_{ij} (r_j(t) + \mu\rho_j(t)), & i \in \Omega_E. \end{cases} \quad (3)$$

The first term on the right side of Eq. (1) for $i \in \Omega_L$ represents the nodes being infected by neighbors within the layers, the second term represents the decreases in s_i due to the departure of the S -state travelers, and the third term describes the increase in s_i due to the arrival of the S -state travelers. In these equations, q is the travel rate of travelers starting from a layer, and $1/t_r$ is the rate of travelers jumping instantaneously from the interlayer edges to a layer. Similarly, for $i \in \Omega_E$ in Eq. (1), the first term represents the change in the S -state nodes due to the infection on the interlayer edges, and the second and third terms, respectively, describe the change in the S -state nodes due to the departure of travelers from the interlayer edges and the arrival of the travelers at the interlayer edges. Equations (2) and (3) describe the dynamics of the infected and recovered nodes, respectively. The probability $\lambda_i(t)$ of an individual being infected by its neighbors at node i at time t is given by

$$\lambda_i(t) = \begin{cases} 1 - \prod_{j=1}^{4N} (1 - \beta c_{ij} \rho_j(t)), & i \in \Omega_L; \\ 1 - \prod_{j=1}^{4N} (1 - \frac{1}{t_r} \alpha \beta c_{ij} \rho_j(t)), & i \in \Omega_E. \end{cases} \quad (4)$$

We have derived the analytical epidemic thresholds using the Jacobian matrix method (Supplementary Note 9).

Spreading dynamics in multilayer network with non-Markovian travel process. Let $s_i^l(t)$, $\rho_i^l(t)$ and $r_i^l(t)$ be the probabilities of i ($i \in \Omega_E$) with travel age l being in the state of S , I , R at time t , respectively. The spreading dynamics in the multilayer system with non-Markovian process can be described as follows.

For $i \in \Omega_L$, we have

$$s_i(t + \Delta t) = (1 - \lambda_i(t)) s_i(t) + q \sum_{j=1}^{4N} d_{ij} (1 - \lambda_j(t)) s_j(t) + \sum_{j=1}^{4N} f_{ij} (1 - \lambda_j^{t_r - \Delta t}(t)) s_j^{t_r - \Delta t}(t); \quad (5)$$

$$\rho_i(t + \Delta t) = (1 - \mu) \rho_i(t) + s_i(t) \lambda_i(t) + q \sum_{j=1}^{4N} d_{ij} [(1 - \mu) \rho_j(t) + s_j(t) \lambda_j(t)] + \sum_{j=1}^{4N} f_{ij} [(1 - \mu) \rho_j^{t_r - \Delta t}(t) + s_j^{t_r - \Delta t}(t) \lambda_j^{t_r - \Delta t}(t)]; \quad (6)$$

$$r_i(t + \Delta t) = r_i(t) + \mu \rho_i(t) + q \sum_{j=1}^{4N} d_{ij} (r_j(t) + \mu \rho_j(t)) + \sum_{j=1}^{4N} f_{ij} (r_j^{t_r - \Delta t}(t) + \mu \rho_j^{t_r - \Delta t}(t)), \quad (7)$$

where the first term on the right side of Eq. (5) represents the S-state nodes not being infected, the second term captures the departure of susceptible travelers from the layers, and the third term describes the arrival of susceptible travelers with travel age $l = t_T - \Delta t$ at the previous time step. Similarly, Eqs. (6) and (7) describe the spreading dynamics of the I and R nodes, respectively.

For $i \in \Omega_E$, we have

$$s_i^l(t + \Delta t) = \begin{cases} (1 - \lambda_i^{l-\Delta t}(t))s_i^{l-\Delta t}(t), \\ l = \Delta t, 2\Delta t, \dots, t_T - \Delta t; \\ q \sum_{j=1}^{4N} f_{ij} (1 - \lambda_j(t))s_j(t), l = 0; \\ 0, l \geq t_T, \end{cases} \quad (8)$$

$$\rho_i^l(t + \Delta t) = \begin{cases} (1 - \mu)\rho_i^{l-\Delta t}(t) + \lambda_i^{l-\Delta t}(t)s_i^{l-\Delta t}(t), \\ l = \Delta t, 2\Delta t, \dots, t_T - \Delta t; \\ q \sum_{j=1}^{4N} f_{ij} [(1 - \mu)\rho_j(t) + s_j(t)\lambda_j(t)], l = 0; \\ 0, l \geq t_T, \end{cases} \quad (9)$$

$$r_i^l(t + \Delta t) = \begin{cases} r_i^{l-\Delta t}(t) + \mu\rho_i^{l-\Delta t}(t), \\ l = \Delta t, 2\Delta t, \dots, t_T - \Delta t; \\ q \sum_{j=1}^{4N} f_{ij} (r_j(t) + \mu\rho_j(t)), l = 0; \\ 0, l \geq t_T. \end{cases} \quad (10)$$

The first case described by Eq. (8) means that the probability of node i in the S-state at time $t + \Delta t$ depends on that of the previous time step, where the current travel age of the travelers is l and their travel age at the previous time step is $l - \Delta t$. The second case in Eq. (8) is that the travelers are about to start their trip with the travel age $l = 0$. The third case is where, when the travel age is equal to or greater than the travel time between the layers, the travelers return to the layers and are not on the interlayer edge. Equations (9) and (10) describe the dynamics of I nodes and R nodes in a similar way.

The probability $\lambda_i(t)$ of an individual being infected at node i in layers by its neighbors at time t is

$$\lambda_i(t) = 1 - \prod_{j=1}^{4N} (1 - \beta c_{ij} \rho_j(t)), i \in \Omega_L, \quad (11)$$

and the probability of a traveler with travel age l being infected at node i on the interlayer edge at time t is

$$\lambda_i^l(t) = 1 - \prod_{j=1}^{4N} (1 - \alpha \beta c_{ij} \rho_j^l(t)) \quad (12)$$

$$, i \in \Omega_E \text{ and } l = 0, \Delta t, \dots, t_T - \Delta t.$$

The number of dynamical equations required to model the spreading dynamics with non-Markovian travel depends on the value of $t_T/\Delta t$.

Data availability

The data that support the findings of this study are available from the corresponding author upon reasonable request.

Code availability

All relevant computer codes are available from the corresponding author upon reasonable request.

Received: 20 September 2022; Accepted: 4 September 2023;

Published online: 20 September 2023

References

- Newman, M. E. Spread of epidemic disease on networks. *Phys. Rev. E* **66**, 016128 (2002).
- Vespignani, A. Predicting the behavior of techno-social systems. *Science* **325**, 425–428 (2009).
- Granell, C., Gómez, S. & Arenas, A. Dynamical interplay between awareness and epidemic spreading in multiplex networks. *Phys. Rev. Lett.* **111**, 128701 (2013).
- Pastor-Satorras, R., Castellano, C., Van Mieghem, P. & Vespignani, A. Epidemic processes in complex networks. *Rev. Mod. Phys.* **87**, 925 (2015).
- Ferguson, N. Capturing human behaviour. *Nature* **446**, 733–733 (2007).
- Funk, S., Salathé, M. & Jansen, V. A. Modelling the influence of human behaviour on the spread of infectious diseases: a review. *J. R. Soc. Interface* **7**, 1247–1256 (2010).
- Brockmann, D. & Helbing, D. The hidden geometry of complex, network-driven contagion phenomena. *Science* **342**, 1337–1342 (2013).
- Buckee, C., Noor, A. & Sattenspiel, L. Thinking clearly about social aspects of infectious disease transmission. *Nature* **595**, 205–213 (2021).
- Barbosa, H. et al. Human mobility: models and applications. *Phys. Rep.* **734**, 1–74 (2018).
- Yan, X.-Y., Zhao, C., Fan, Y., Di, Z.-R. & Wang, W.-X. Universal predictability of mobility patterns in cities. *J. R. Soc. Interface* **11**, 20140834 (2014).
- Zhao, Y.-M., Zeng, A., Yan, X.-Y., Wang, W.-X. & Lai, Y.-C. Unified underpinning of human mobility in the real world and cyberspace. *N. J. Phys.* **18**, 053025 (2016).
- Yan, X.-Y., Wang, W.-X., Gao, Z.-Y. & Lai, Y.-C. Universal model of individual and population mobility on diverse spatial scales. *Nat. Commun.* **8**, 1639 (2017).
- Balcan, D. et al. Multiscale mobility networks and the spatial spreading of infectious diseases. *Proc. Natl Acad. Sci. USA* **106**, 21484–21489 (2009).
- Arenas, A. et al. Modeling the spatiotemporal epidemic spreading of COVID-19 and the impact of mobility and social distancing interventions. *Phys. Rev. X* **10**, 041055 (2020).
- Chang, S. et al. Mobility network models of COVID-19 explain inequities and inform reopening. *Nature* **589**, 82–87 (2021).
- De Domenico, M., Solé-Ribalta, A., Gómez, S. & Arenas, A. Navigability of interconnected networks under random failures. *Proc. Natl Acad. Sci. USA* **111**, 8351–8356 (2014).
- Bianconi, G. *Multilayer Networks: Structure and Function* (Oxford University Press, 2018).
- Wang, L. & Wu, J. T. Characterizing the dynamics underlying global spread of epidemics. *Nat. Commun.* **9**, 1–11 (2018).
- Alessandretti, L. What human mobility data tell us about COVID-19 spread. *Nat. Rev. Phys.* **4**, 12–13 (2022).
- Rvachev, L. A. & Longini Jr, I. M. A mathematical model for the global spread of influenza. *Math. Biosci.* **75**, 3–22 (1985).
- Hufnagel, L., Brockmann, D. & Geisel, T. Forecast and control of epidemics in a globalized world. *Proc. Natl Acad. Sci. USA* **101**, 15124–15129 (2004).
- Colizza, V., Pastor-Satorras, R. & Vespignani, A. Reaction–diffusion processes and metapopulation models in heterogeneous networks. *Nat. Phys.* **3**, 276–282 (2007).
- Keeling, M. J., Danon, L., Vernon, M. C. & House, T. A. Individual identity and movement networks for disease metapopulations. *Proc. Natl Acad. Sci. USA* **107**, 8866–8870 (2010).
- Belik, V., Geisel, T. & Brockmann, D. Natural human mobility patterns and spatial spread of infectious diseases. *Phys. Rev. X* **1**, 011001 (2011).
- Gómez-Gardeñes, J., Soriano-Paños, D. & Arenas, A. Critical regimes driven by recurrent mobility patterns of reaction–diffusion processes in networks. *Nat. Phys.* **14**, 391–395 (2018).
- Chinazzi, M. et al. The effect of travel restrictions on the spread of the 2019 novel coronavirus (COVID-19) outbreak. *Science* **368**, 395–400 (2020).
- Gomez, S. et al. Diffusion dynamics on multiplex networks. *Phys. Rev. Lett.* **110**, 028701 (2013).
- De Domenico, M., Granell, C., Porter, M. A. & Arenas, A. The physics of spreading processes in multilayer networks. *Nat. Phys.* **12**, 901–906 (2016).
- Kivela, M. et al. Multilayer networks. *J. Complex Net.* **2**, 203–271 (2014).
- Saunell-Mendiola, A., Serrano, M. Á. & Boguná, M. Epidemic spreading on interconnected networks. *Phys. Rev. E* **86**, 026106 (2012).
- Wu, D., Tang, M., Liu, Z. & Lai, Y.-C. Impact of inter-layer hopping on epidemic spreading in a multilayer network. *Commun. Nonlinear Sci. Numer. Simul.* **90**, 105403 (2020).

32. Choi, E. M. et al. In-flight transmission of SARS-CoV-2. *Emerg. Infect. Dis.* **26**, 2713 (2020).
33. Hu, M. et al. Risk of coronavirus disease 2019 transmission in train passengers: an epidemiological and modeling study. *Clin. Infect. Dis.* **72**, 604–610 (2021).
34. Tsuchihashi, Y. et al. High attack rate of SARS-CoV-2 infections during a bus tour in Japan. *J. Travel Med.* **28**, taab111 (2021).
35. Bai, Y., Huang, Q. & Du, Z. Measuring the impact of public transit on the transmission of epidemics. *International Conference on Mobile Wireless Middleware, Operating Systems, and Applications*, 104–109 (Springer, 2020).
36. Li, T. Simulating the spread of epidemics in China on multi-layer transportation networks: beyond COVID-19 in Wuhan. *Europhys. Lett.* **130**, 48002 (2020).
37. Mo, B. et al. Modeling epidemic spreading through public transit using time-varying encounter network. *Transp. Res. C Emerg. Technol.* **122**, 102893 (2021).
38. Qian, X. & Ukkusuri, S. V. Connecting urban transportation systems with the spread of infectious diseases: a Trans-SEIR modeling approach. *Transp. Res. B Methodol.* **145**, 185–211 (2021).
39. Barabasi, A.-L. The origin of bursts and heavy tails in human dynamics. *Nature* **435**, 207–211 (2005).
40. Gonzalez, M. C., Hidalgo, C. A. & Barabasi, A.-L. Understanding individual human mobility patterns. *Nature* **453**, 779–782 (2008).
41. Boguná, M., Lafuerza, L. F., Toral, R. & Serrano, M. Á. Simulating non-Markovian stochastic processes. *Phys. Rev. E* **90**, 042108 (2014).
42. Van Mieghem, P. & Van de Bovenkamp, R. Non-Markovian infection spread dramatically alters the susceptible-infected-susceptible epidemic threshold in networks. *Phys. Rev. Lett.* **110**, 108701 (2013).
43. Kiss, I. Z., Röst, G. & Vizi, Z. Generalization of pairwise models to non-Markovian epidemics on networks. *Phys. Rev. Lett.* **115**, 078701 (2015).
44. Starnini, M., Gleeson, J. P. & Boguñá, M. Equivalence between non-Markovian and Markovian dynamics in epidemic spreading processes. *Phys. Rev. Lett.* **118**, 128301 (2017).
45. Feng, M., Cai, S.-M., Tang, M. & Lai, Y.-C. Equivalence and its invalidation between non-Markovian and Markovian spreading dynamics on complex networks. *Nat. Commun.* **10**, 1–10 (2019).
46. Lin, Z.-H. et al. Non-Markovian recovery makes complex networks more resilient against large-scale failures. *Nat. Commun.* **11**, 1–10 (2020).
47. Castellano, C. & Pastor-Satorras, R. Thresholds for epidemic spreading in networks. *Phys. Rev. Lett.* **105**, 218701 (2010).
48. Liu, Q.-H., Wang, W., Tang, M. & Zhang, H.-F. Impacts of complex behavioral responses on asymmetric interacting spreading dynamics in multiplex networks. *Sci. Rep.* **6**, 1–13 (2016).
49. Pastor-Satorras, R. & Vespignani, A. Epidemic spreading in scale-free networks. *Phys. Rev. Lett.* **86**, 3200–3203 (2001).
50. Pastor-Satorras, R. & Vespignani, A. Epidemic outbreaks in complex heterogeneous networks. *Eur. Phys. J. B* **26**, 521–529 (2002).
51. Shu, P., Wang, W., Tang, M., Zhao, P. & Zhang, Y. C. Recovery rate affects the effective epidemic threshold with synchronous updating. *Chaos* **26**, 063108 (2016).
52. Fennell, P. G., Melnik, S. & Gleeson, J. P. Limitations of discrete-time approaches to continuous-time contagion dynamics. *Phys. Rev. E* **94**, 052125 (2016).
53. Keeling, M. J. & Rohani, P. *Modeling Infectious Diseases in Humans and Animals* (Princeton University Press, 2011).
54. Radicchi, F. & Castellano, C. Beyond the locally treelike approximation for percolation on real networks. *Phys. Rev. E* **93**, 030302 (2016).

Acknowledgements

This work is supported by the National Natural Science Foundation of China (Nos. 61802321, 12231012 and 11975099), Sichuan Science and Technology Program (No. 2020YJ0125), the Southwest Petroleum University Innovation Base (No. 642) and the Science and Technology Commission of Shanghai Municipality (No. 22DZ2229004). The work at Arizona State University was supported by the Office of Naval Research through Grant No. N00014-21-1-2323.

Author contributions

Y.C., Y.L., M.T. and Y.-C.L. designed research; Y.C. performed calculations and numerical simulations; Y.C., Y.L. and M.T. contributed analytic tools; Y.C., Y.L., M.T. and Y.-C.L. analyzed data; Y.C., Y.L., M.T. and Y.-C.L. wrote the paper.

Competing interests

The authors declare no competing interests.

Additional information

Supplementary information The online version contains supplementary material available at <https://doi.org/10.1038/s42005-023-01369-9>.

Correspondence and requests for materials should be addressed to Ying Liu or Ming Tang.

Peer review information *Communications Physics* thanks Fredrick Dahlgren and the other anonymous reviewers for their contribution to the peer review of this work.

Reprints and permission information is available at <http://www.nature.com/reprints>

Publisher's note Springer Nature remains neutral with regard to jurisdictional claims in published maps and institutional affiliations.



Open Access This article is licensed under a Creative Commons Attribution 4.0 International License, which permits use, sharing, adaptation, distribution and reproduction in any medium or format, as long as you give appropriate credit to the original author(s) and the source, provide a link to the Creative Commons licence, and indicate if changes were made. The images or other third party material in this article are included in the article's Creative Commons licence, unless indicated otherwise in a credit line to the material. If material is not included in the article's Creative Commons licence and your intended use is not permitted by statutory regulation or exceeds the permitted use, you will need to obtain permission directly from the copyright holder. To view a copy of this licence, visit <http://creativecommons.org/licenses/by/4.0/>.

© The Author(s) 2023